PAPER REFERENCE: **3M.153**

NUMERICAL MODELLING OF CYCLIC STRESS-STRAIN FIELDS NEAR A CRACK TIP: THE ROLE OF STRAIN HARDENING

J. Toribio[1] and V. Kharin[2]

[1]Materials Science Department, University of La Coruiia, ETSI Caminos, 15071 La Coruiia, Spain
[2]Mechanical and Civil Engng. Department, University of Salamanca, Campus Viriato, 49022 Zamora, Spain

ABSTRACT

Finite-element large deformation analysis of the cracked strain-hardening elastoplastic solid under cyclic loading was performed. Minor quantitative changes, but not essential distinctions, were found in the near tip stress fields comparing the data corresponding to different hardening rules (isotropic, kinematic and mixed) with the perfectly-plastic constitutive model. As regards the deformations, strain-hardening facilitates formation of the localised slip bands near the crack tip, and this localisation of plasticity is strongly promoted by the kinematic component of the hardening. This causes accelerated accumulation of plastic strain in certain locations. The implications of the results for fatigue crack growth are discussed.

INTRODUCTION

Analyses of the crack tip stress and deformation fields are essential for understanding of the crack propagation phenomena and for development of adequate predictive tools by means of linking relevant stress-strain characteristics to microscopical rupture mechanisms. Several high-resolution studies of the crack tip fields have been performed taking into account both constitutive (plasticity) and geometrical (large deformations) nonlinearities which are equally essential to gain realistic implications for fracture [1,2]. The monotonic loading situations have received extensive consideration there. In relation to fatigue, studies accounting for the roles of plasticity and large geometry changes have been performed mostly for the perfectly-plastic material [3,4]. However, only limited data have been generated till now considering more realistic material behaviours including strain hardening [5,6].

In this contribution the effect of the strain-hardening on the near-tip situation under cyclic loading is addressed. Finite deformation elastoplastic simulations were performed for both strain-hardening and perfectly-plastic solids under plane-strain mode I (opening) cyclic loading. Small scale yielding conditions were ensured to allow the linear elastic fracture mechanics variable — the stress intensity factor K — to be the controlling parameter of the crack tip situation irrespective of the geometry of the solid and distribution of applied loads.

DESIGN OF THE MODEL

Material

The model of perfectly-plastic solid, although suitable for analytical and numerical evaluations, does not accurately represent the response of materials which usually manifest strain hardening. It may be expected to improve the approximation adopting the controlling material parameter to be not simply a conventional engineering 0.2% offset yield strength $\sigma_{0.2}$, but a suitable effective value of the yield stress σ_Y as modified by strain hardening [7]. Then, owing to the similitude of the corresponding elastoplastic solutions with respect to σ_Y and the dimensionless factor σ_Y/E, where E is the Young modulus, strain hardening of materials may affect only the scaling of the established stress-strain fields [1-3], but not their shape, under otherwise similar geometry-and-loading circumstances.

It is clear that "irrespective of the method of solution, the results of an elastic-plastic analysis are as good as the constitutive model employed" [8]. While certain model deficiencies may not substantially alter the results in

many analysis tasks, usually it is not easy to perceive a ***priori*** if a model in use would not miss important features of the stress-strain fields in question. In relation to the crack tip, it seems useful to consider various constitutive models focusing on their possible effects on the crack tip situation during fatigue.

The rate-independent strain-hardening elastoplastic solid with von Mises yield surface was considered in this paper. Mechanical characteristics of the material correspond to the experimental data for a cold-drawn high-strength steel [9] as follows: E = 195 GPa, Poisson ratio $\nu = 0.3$, $\sigma_{0.2}$ = 1500 MPa, and fracture toughness $K_{IC} = 84\ \mathrm{MPa \cdot m^{1/2}}$. The monotonic-loading stress-strain curve of the steel is approximated by the Ramberg-Osgood equation which relates the equivalent plastic strain ε_{eq}^{p} to the equivalent stress σ_{eq} as follows:

$$\varepsilon_{eq}^{p} = \left(\frac{\sigma_{eq}}{S}\right)^{n} \tag{1}$$

where the hardening exponent and the strength coefficient respectively are n = 17 and S = 2160 MPa. As a complementary, the model of perfectly-plastic solid was implemented for this prototype material taking the effective yield ("flow") stress σ_Y instead of conventional yield strength $\sigma_{0.2}$ as suggested by Rice to adjust the results about strain-hardening and perfectly plastic crack tip fields under monotonic loading (cf. [1,10]):

$$\sigma_Y = \sigma_{0.2}\left[\frac{2}{\sqrt{3}}(1+\mu)(1+n)\,\frac{\sigma_{0.2}}{E}\right]^{-1/n} \tag{2}$$

With the cited material parameters this yields σ_Y = 1645 MPa.

The simple approaches to handle strain-hardening with a single yield surface are the isotropic, the kinematic and the combined isotropic-to-kinematic hardening rules. Although they are limited as regards the ability to rationalise typical cyclic plasticity phenomena **[11],** such as cyclic softening, ratcheting, etc., they are chosen as the first step to elucidate the strain-hardening effects near the crack tip under cyclic loading. In the simulations, apart from the perfect plasticity, three kinds of hardening rules were tried: isotropic, kinematic and mixed (intermediate) one, all them based on the same stress-strain curve given by Eqn. 1.

Geometry and loading

Confining the analysis to K-controlled small-scale yielding situation, model geometry and loading were taken the same as in the perfect plasticity simulations [3,4]. The double-edge-cracked panel under tensile stresses σ_{app} was considered (Figure 1). The undeformed crack of the length a = 75 mm had parallel flanks and smooth round-shape tip. The crack width (twice the radius) in the main body of simulations was b_0 = 5 pm, although in some trials half this value was taken. The simulated loading regime was cycling between zero load and constant maximum stress intensity factor $K_{max} = 0.6K_{IC}$. Loading pattern $\sigma_{app}(t)$ was taken of a sine-like shape with maxima at odd times $t = 2k - 1$ and minima at even $t = 2k$ in the k-th load cycle $(k = 1,2,...)$.

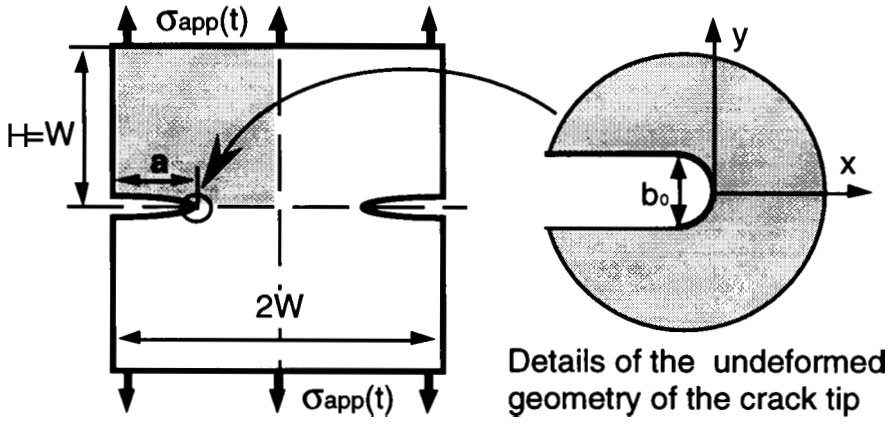

Figure 1: The model testpiece geometry and applied load.

Procedure

The nonlinear finite-element code MARC was employed with updated Lagrangian formulation to perform large displacements—large strains elastoplastic analysis. Owing to symmetry, calculations were carried out for the one-quarter **of** the panel (shadowed on the testpiece scheme in Figure 1). Usually, the intention was to accomplish several loading cycles, typically up to ten. However, the simulations were often terminated by the

finite-element mesh degeneration. To achieve longer loading histories, the near tip mesh and the load stepping procedure of the solution had to be finer than in similar studies of the monotonic loading of strain-hardening solids or cycling of the perfectly-plastic material **[l-51.** Various meshes of four-node quadrilateral finite elements were tried. The optimum mesh of **2189** elements, **2284** nodes and the smallest element mean dimension $0.016b_0$ was chosen. The number of load steps between load extremes was typically **200,** but in some trials the number was taken to be **300.**

RESULTS

Under coarse examination, cyclic crack tip fields for all tried hardening rules —isotropic, kinematic and mixed one— display affinity between them and also agree with the data for the perfectly-plastic material, these latter being essentially the same as described elsewhere **[3,4]**. However, at higher resolution substantial distinctions are revealed which advance with plastic strain accumulation, and the kind of strain hardening seems to be responsible for their development.

Crack Tip Deformation

For all considered strain-hardening rules, the crack tip profiles and nearby deformation evolve in a qualitatively similar manners, but with increasing differentiation between them and the perfectly plastic case whilst loading *goes* on. At the initial stages of loading, the tip shapes remained smoothly-round and similar to the observed in a perfectly-plastic solid **[3,4]**. However, whilst loading continues, the smoothly curved tip acquires a cornered shape (Figure **2).** This is accompanied by development of the shear bands from these comers towards material interior, and appearance of the wedge-shaped region in front of the tip apex which undergoes little deformation since then. The localised deformation sooner or later, depending on the kind of hardening, distorts drastically the finite-element mesh which eventually collapses. This impedes to go on with further modelling. With the adopted mesh design, the simulation with the kinematic hardening rule terminated in the third cycle of loading, whereas the isotropic hardening solid endured till eight cycles, and the perfectly-plastic one even more.

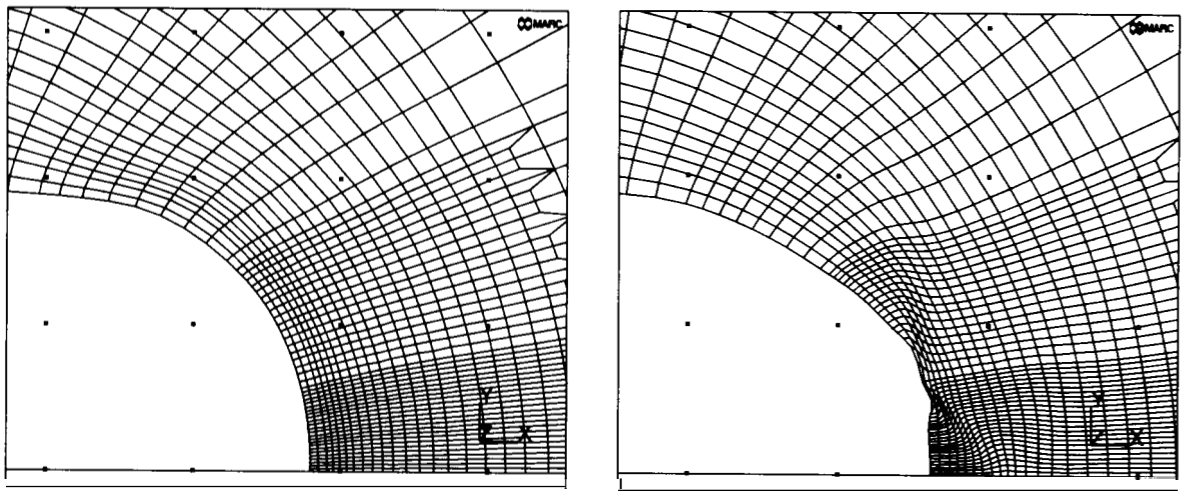

Figure 2: Crack tip deformations at load approaching the maximum level, $K = 0.86K_{max}$, in the third cycle for the perfectly plastic (the left-hand picture) and kinematic strain-hardening (the right-hand one) material behaviour (grid spacing on both pictures is equal to **bd2 =**2.5 pm).

Analogous phenomenon of the vertex formation on the tip contour and penetration of the localised shear bands beyond the tip was observed under monotonic load for the material with a corner (non-Mises) flow theory and isotropic power-law strain-hardening, but it was not detected when smooth (von Mises) flow surface was in use with otherwise the same characteristics of plastic behaviour **[2].** Now quite similar effect occurs with smooth von Mises yield surface under cyclic loading. It seems that plastic flow localisation is a general phenomenon although, to observe it, notable development requires to exceed some level of strain depending on a certain constitutive model (flow surface and hardening rule). In particular, these localisations of deformation out of the crack plane are strongly promoted by the kinematic component of the hardening. Along the same load pattern, at more kinematic hardening, changing from the isotropic to the pure kinematic one, the tip cornering and strain localisation started at lower cycles number N and developed faster. The vortex location on the tip profile seems to be associated with the initial crack width (its tip radius) *bo:* in calculations with $b_0/2$ = *2.5* and 5 pm with otherwise the same model parameters, the material point where the vortex appeared was

apparently the same with respect to its location on the undeformed crack tip contour. Obviously, the actual position of this material point in the deformed solid configuration depends on the applied load level.

Near Tip Stress Fields

In spite of a notable effect of the strain hardening (or its absence) on the kinematics of the near tip deformation, only minor distinctions can be found comparing the stress fields in strain-hardening materials with the data for the perfectly-plastic model **[3,4]**. The spatial distributions of the maximum principal stress σ_1 for all strain-hardening behaviours are quite similar between them and the perfectly plastic case, as shown in the examples of Figure **3.** The minor local disturbances may be detected in a strain-hardening materials as a slight ridge of the stress distribution associated with the shear band, which arise on the later stages of deformation together with the described localisation of deformation.

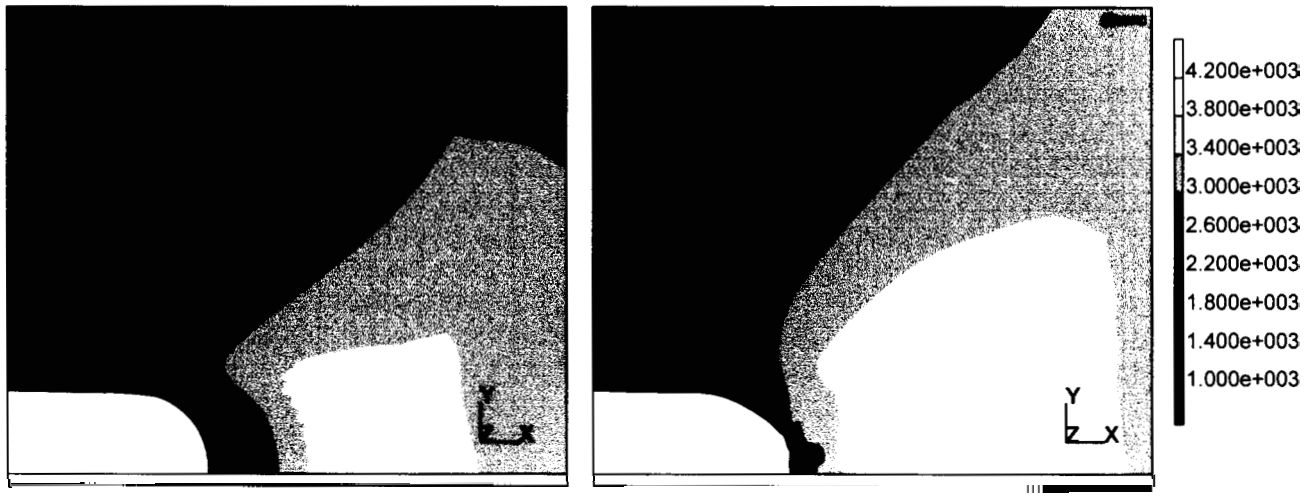

Figure 3: Maximum principal stress (MPa) at load approaching the maximum level, $K = 0.86K_{max}$, in the third cycle for the cases of perfectly plastic (the left-hand picture) and kinematic strain-hardening (the right-hand one) material constitutive model.

The peculiarities of the distributions of the principal stress along the crack line, i.e. of the axial stress $\sigma_1 = \sigma_{yy}$, against the deformed distance from the tip apex $x > 0$ (the coordinate system is shown in Figure 1), are displayed in Figure **4.** Again, minor perturbations of the stress pattern appear very close to the crack tip, such as a minute peak at the intersection of the symmetrical shear bands on the crack axis.

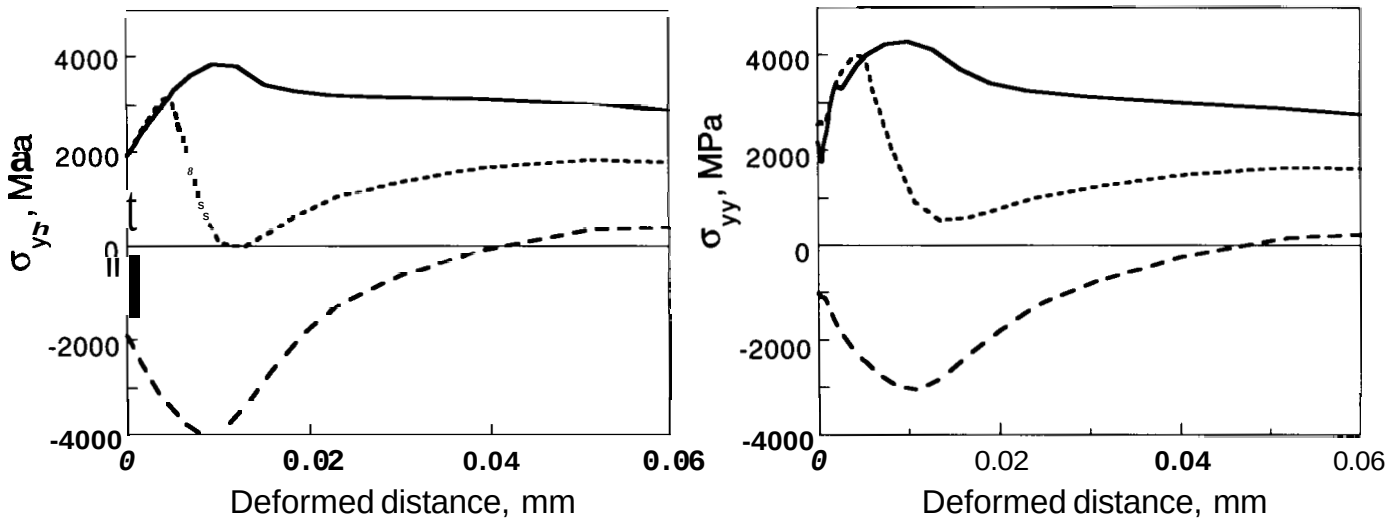

Figure 4: The stress $\sigma_{yy}(x)$ in the deformed configuration in the third loading cycle for the perfectly plastic (the left-hand picture) and kinematic strain-hardening (the right-hand one) materials; dashed line: at unloading (applied $K = 0$); dotted line: at forward loading on the mid-way towards the top level ($K = 0.5K_{max}$); solid line: at forward loading approaching the maximum ($K = 0.86K_{max}$).

With regard to the stress evolutions in selected material points, they follow along rather similar patterns for all considered constitutive behaviours and display nearly constant-amplitude trajectories with no substantial dependence on the cycle number (Figure **5)**. The role of strain hardening is mainly the alteration of the stress ratio in a material point X — the ratio the minimum stress to the maximum one of the cycle, $R = \sigma_{min}/\sigma_{max}$. This effect diminishes with the distance from the tip (cf. the curves for the points $X_1 < X3$ in Figure **5)**.

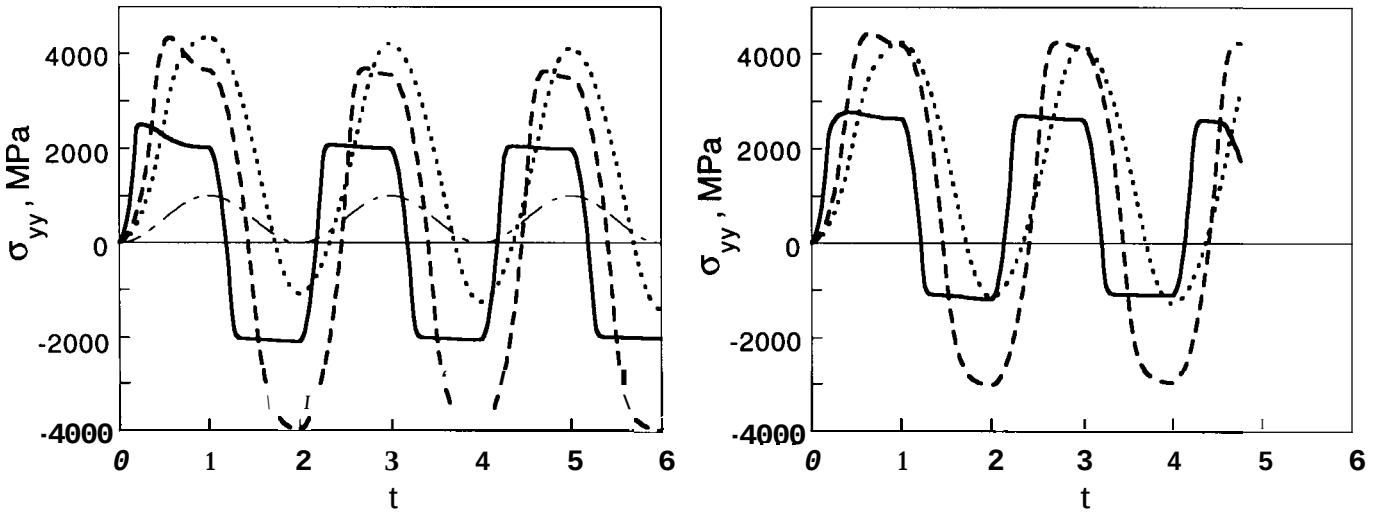

Figure 5: Stress evolutions $\sigma_{yy}(t)$ under sine-shape pattern of the applied loading (shown by the dash-and-dot curve in arbitrary units in the left-hand picture) for the perfectly plastic (to the left) and kinematic strain-hardening (to the right) solids in the material points X ahead of the crack tip identified by their distances from the tip apex in the undeformed configuration; solid line: at $X_1 = 0.2b_0$; dashed line: at $X_2 = 2.1b_0$; dotted line: at $X3 = 5.3b_0$.

Crack Tip Plastic Strains

Strain-based variables are often used as measures of damage accumulation in fatigue [11]. They are the actual equivalent plastic strain ε_{eq}^p and the total (cumulative) equivalent plastic strain ε_{tot}^p defined along a specific path of the plastic strain evolution, expressed in terms of the plastic strain components ε_{ij}^p, respectively, as follows:

$$\varepsilon_{eq}^p = \left(\frac{2}{3}\varepsilon_{ij}^p \varepsilon_{ij}^p\right)^{1/2} \quad \left(\text{where } \varepsilon_{ij}^p = \int d\varepsilon_{ij}^p\right) \quad \text{and} \quad \varepsilon_{tot}^p = \int\left(\frac{2}{3} d\varepsilon_{ij}^p d\varepsilon_{ij}^p\right)^{1/2} \tag{3}$$

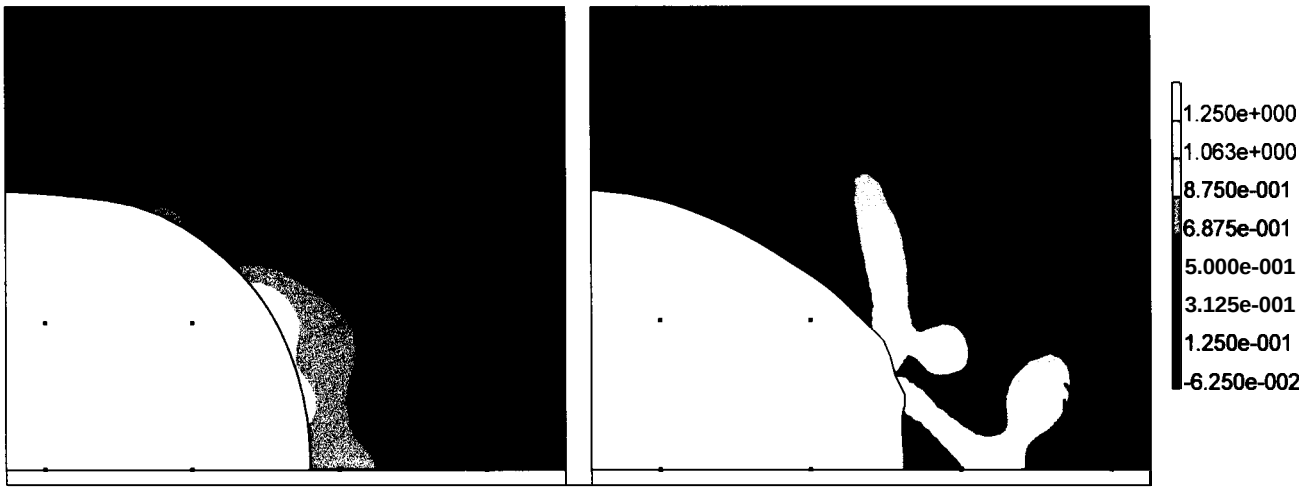

Figure 6: Equivalent plastic strain rate $d\varepsilon_{eq}^p/dt$ (arbitrary units) at load approaching the maximum level, $K = 0.86K_{max}$, in the third cycle for the perfectly plastic (the left-hand picture) and kinematic strain-hardening (the right-hand one) material constitutive models.

The evolution of strain distribution near the crack tip is better displayed using the equivalent plastic strain rate $d\varepsilon_{eq}^p/dt$ as a sensitive indicator of the progressing strain concentration and localisation. Generated contour band plots of $d\varepsilon_{eq}^p/dt$, like examples shown on Figure ***6***, reveal that even under monotonic loading the peak of the strain concentration, initially located at the tip apex on the symmetry axis of the crack, splits whilst load increases, ***so*** that two loci of plastic strain accumulation appear out of the tip apex at apparently fixed symmetric positions in respective specimen halves above and beneath the symmetry axis of the crack. This is qualitatively common for all material behaviours, including perfect plasticity.

Meanwhile, the presence of hardening and especially its kind (isotropic or kinematic) cause substantial quantitative distinctions. In the perfectly-plastic material, these concentrations of the plastic strain remain mild and slowly developing with continuing loading (left-hand drawing in Figure ***6)***. In contrast, strain-hardening makes these strain concentrations quite more steep (more localised), promotes their faster development to form the sharply localised shear bands when changing from perfect plasticity through isotropic hardening towards kinematic one for which the strain accumulation peak becomes the most acute. With perfect plasticity or isotropic hardening these separated maxima of the plastic strain are quite round and wide so their detection needs higher resolution than that used in the previous studies of monotonically loaded crack, such as [1,2]. On the other hand, the kinematic hardening produces the sharpest localised shear bands, and their revealing in simulations requires refinement of the finite element mesh. In general, strain localisation near the crack tip arises under both monotonic and cyclic loadings and seems to be driven by increase of the actual or cumulative plastic strain, although the rate of its development depends strongly on a specific kind of hardening.

Plastic strain distributions in the crack plane ahead of the tip depending on the material point distance from the tip in the deformed configuration (Figure 7) display quite large perturbations due to strain hardening if compared with those of the stress field. The sharp peaks there manifest the plastic strain localisation and concentration in the shear bands, and they mark possible locations of the strain controlled local fracture nuclei.

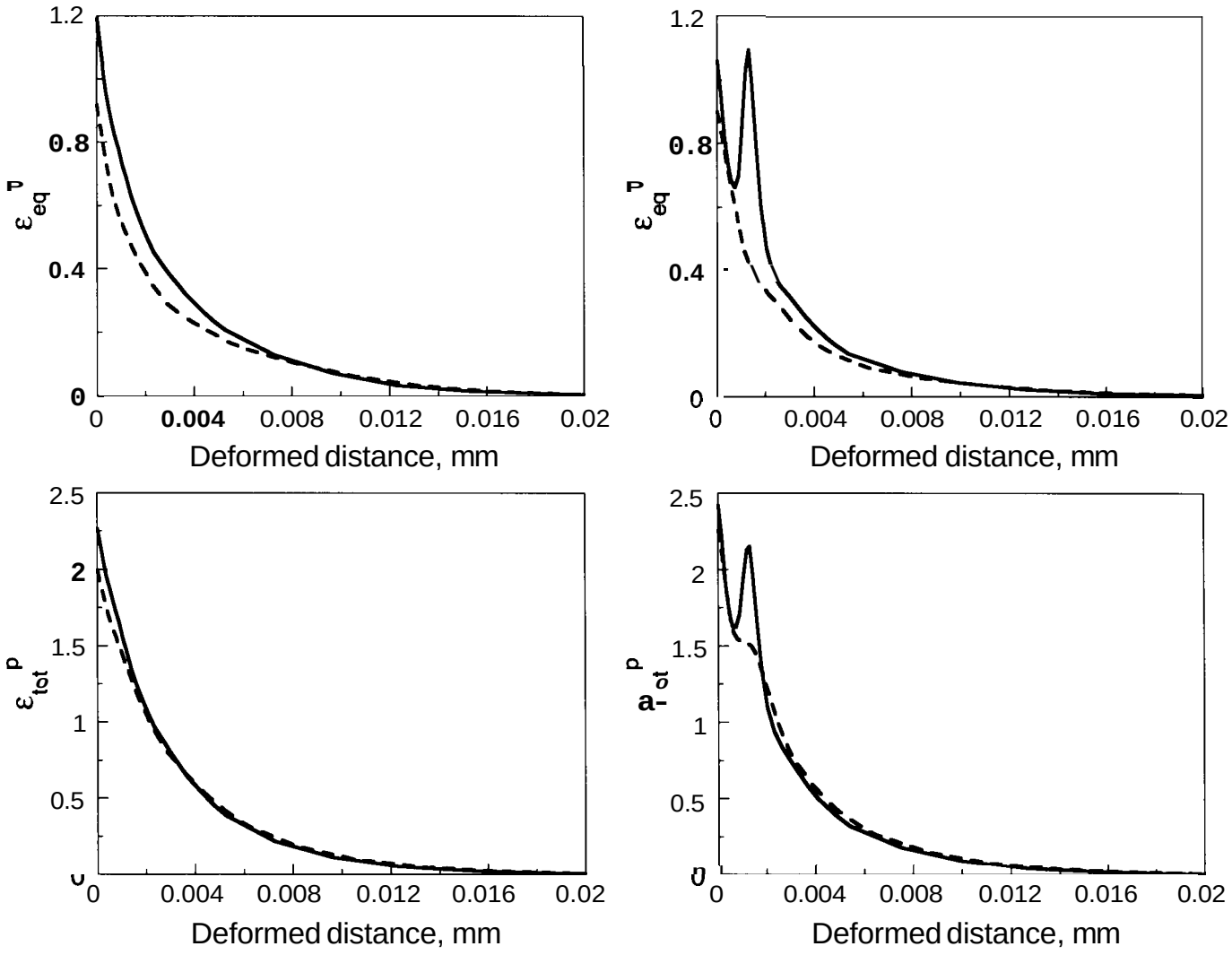

Figure 7: Plastic strains $\varepsilon_{eq}^p(x)$ and $\varepsilon_{tot}^p(x)$ in the deformed configuration in the third loading cycle for the perfectly plastic (to the left) and kinematic strain hardening (to the right) materials; dashed line: at $K = 0$; solid line: at forward loading towards the maximum, $K = 0.86K_{max}$.

With regard to the evolution of plastic strains, both plastic strain measures $\varepsilon_{eq}^{p}(t)$ and $\varepsilon_{tot}^{p}(t)$ increase with apparently constant averaged rates per cycle $d\varepsilon_{eq,tot}^{p}/dN$ provided strain localisation has not started yet. After shear bands creation, the elevation of both $d\varepsilon_{eq,tot}^{p}$ accelerates sharply within the bands, delays in the wedge-shaped domain between them (Figure 8), and maintains a fairly constant rate per cycle outside the zone affected by the strain localisation.

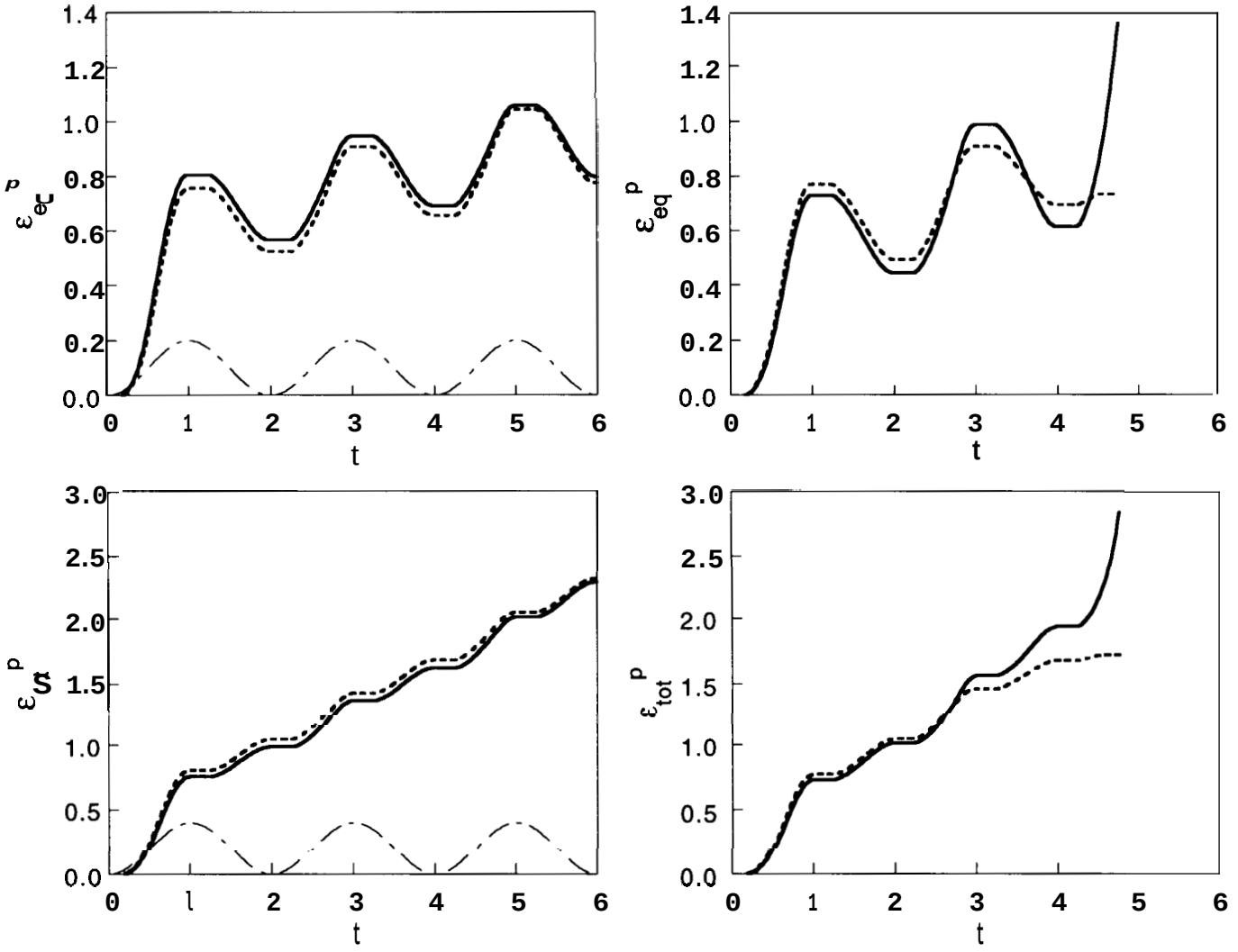

Figure 8: Typical evolutions of the plastic strains ε_{eq}^{p} and ε_{tot}^{p} in the material points $X_{1,2}$ located initially at approximately the same depth of $0.2b_0$ from the crack tip surface under sine-shape pattern of the applied loading route (shown by the dash-and-dot curve in arbitrary units) for the perfectly plastic (to the left) and kinematic strain-hardening (to the right) materials; the point X_1 belongs to the crack plane and remains in the wedge-shaped domain between the shear bands (when they arise), and the point X_2 is out of the crack plane and belongs to the shear band (where it appears).

DISCUSSION

Some implications may be derived from the reported results with regard to the role of strain hardening in fatigue. The local criteria for crack advance are usually derived by means of association of the local rupture event with some critical condition in terms of local stress, strain, or both as governing factors [8,11]. Modelling shows that the stress fields in the supposed fracture process zone near the crack tip are nearly insensitive to the material hardening. In all simulated cases, stresses oscillated in a nearly constant-amplitude manner in respective material points. In contrast, the plastic strain fields are notably sensitive to the strain hardening, and especially to the strength of the Bauschinger effect associated with the kinematic portion of the hardening. This kinematic hardening component strongly promotes early localisation of the crack tip plasticity within narrow bands where the current and total plastic strains increase sharply when loading goes on.

With any kind of the strain-hardening, in contrast to apparently constant-amplitude stress history (Figure 5), the near tip plastic strain field intensities increase: the oscillating current plastic strain ε_e manifests cyclic ratcheting, whereas the cumulative one ε_{tot}^{p} shows monotonic climbing (Figure 8). At any rate, being

increasing functions of the number of the loading cycles, each of them can serve as the measure of the approaching locally the limit state in fatigue. Then the criterion of critical strain - either current or total (cumulative) — as the condition of the local rupture seems to be promising to predict fatigue crack growth rates under various cyclic loading regimes.

As regards the role of the strain hardening, enhancement of the strain localisation by the kinematic component of hardening seems to be a promoter of the fatigue damaging or local exhausting of the strain accommodation capability of the material. Formation of the shear bands implies the possibility of some microfracture mechanism to be operative ahead of the crack tip at the intersection of the persistent slip planes. This indicates possible locations of the nucleus of crack-tip rupture. In due course, their depth ahead of the crack tip may be associated with the fatigue striations. On the other hand, these localised shear bands can act as the decohesion planes to form the serrated profile of the crack growth path. Both these formations are obviously observed on fatigue fracture surfaces [11], so that the performed modelling seems to be able to reproduce the notable features of the fatigue crack growth.

CONCLUSIONS

High resolution large-deformation finite-element analysis of a cyclic loading of the stationary plane-strain crack in elastoplastic material with various kinds of strain hardening reveals the substantial role of the kind of the hardening —kinematic or isotropic — on the evolution of the crack tip deformation and plastic strain fields with minor influence on the stress state therein. This latter turns out to be nearly constant amplitude stress cycling with variable stress ratio depending on the position of the material point.

The important feature of the plastic strain fields is the trend to strain localisation aside from the plane of the crack and formation of the shear bands. Strain hardening affects substantially the bands development which appears to be strongly promoted by the kinematic portion of the strain hardening. Accelerated increase of the actual as well as of the total (cumulative) plastic strains in these bands when loading goes on makes them the preferable sites of the eventual local rupture. This seems to be consistent with the frequently observed formation of fatigue striations and serrated profile of the fatigue crack surface.

As far as both measures of the plastic strain evolution near the crack tip —the actual and the total equivalent plastic strains — are rising functions of the load cycle number, each of them is potentially capable to be the controlling variable for the advancement of the fatigue damage, approaching the limit state and eventual local rupture at the crack tip. This creates a basis for linking stress-strain analysis with rupture micromechanisms and development of the predictive tools with regard to the fatigue crack extension.

Acknowledgement
This work was funded by the Spanish CICYT (Grant MAT97-0442) and Xunta de Galicia (Grants XUGA 11801B95 and XUGA 11802B97). One of the authors (VKh) is indebted to the University of A Coruña and *Xunta de Galicia* who anabled this study, and to the University of Salamanca for facilitation of its termination.

REFERENCES

1. McMeeking, R.M. (1977) *J. Mech. Phys. Solids* **25,** 357.
2. Needleman, A. and Tvergaard, V. (1983). In: *Elastic-Plastic Fracture: Second Symposium. Vol. I — Inelastic Crack Analysis, ASTM STP 803,* pp. 80–115, Philadelphia.
3. Toribio, J. and Kharin, V. (1998). In: *Fracturefrom Defects, Proc. 12th Eur. Con. Fracture,* pp. 1059–1064, EMAS, Warley.
4. Toribio, J. and Kharin, V. (1999). In: *Advances in Fatigue Crack Closure Measurement and Analysis: Second Volume, ASTM STP 1343,* pp. 440-458, West Conshohocken.
5. Gortemaker, P.C.M., de Pater, C. and Spiering R.M.E.J. (1981). In: *Proc. 5th Int. Con. Fracture,* pp. 151–160, Pergamon Press, Oxford.
6. Toribio, J. and Kharin, V.(1998) *J. Mech. Behav. of Mater.* **9,** 205.
7. Rice, J.R. (1967). In: *Fatigue Crack Propagation, ASTM STP 415,* pp. 247-309, Philadelphia.
8. Ellyin, F. and Wu, J.(1992) *Int. J. Fracture* ***56,*** 189.
9. Toribio, J. and Lancha, A.M. (1993) *Materials and Structures* **26,** 30.
10. Rice, J.R., McMeeking, R.M., Parks, D.M. and Sorensen, E.P. (1979) Comp. Meth. Appl. Mech. Eng. **17/18,** 411.
11. Suresh, S. (1991). *Fatigue of Materials.* Cambridge University Press.